POLARIMETRIC SCATTERING SIMULATION AND DATA/IMAGE INFORMATIOIN ANALYSIS FOR ALOS PALSAR AND AIRBORNE PISAR IMAGES

Ya-Qiu Jin [(1)] PI No 310
Co-Investigators *Motoyuki Sato* [(2)], *Koichi Iribe* [(2)]

[(1)] Key Lab of Wave Scattering and Remote Sensing Information
Fudan University, Shanghai 200433, China
E-mail: yqjin@fudan.ac.cn Tel/Fax : 86-21-65643902

[(2)] Tohoku University, Japan
E-mail: sato@cneas.tohoku.ac.jp iribe@cneas.tohoku.ac.jp

1. INTRODUCTION

A model of polarimetric scattering from a layer of vegetation canopy with snow coverage is developed, as shown in Fig. 1[1]. The vegetation canopy is modeled as a layer of non-spherical (spheroid leaves, branches and trunk cylinders) scatterers, and the snowpack is modeled as a layer of dense spherical ice grains. Numerical simulation of polarimetric scattering, $\sigma_{hh}, \sigma_{vv}, \sigma_{hv}, \sigma_{vh}$, and some characteristic functions, e.g. H and α in decomposition theorem, are applied to data/image analysis of ALOS PALSAR and airborne PISAR at L and X bands.
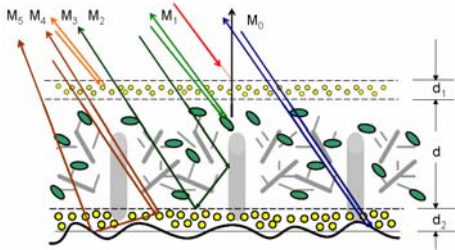

Fig. 1 Model of snow covered forestry

2. MUELLER MATRIX SOLUTION

As shown in Fig. 1, the Mueller matrix solution is presented as [2,3]

$$\overline{\mathbf{M}} = \overline{\mathbf{M}}_0 + \overline{\mathbf{M}}_1 + \overline{\mathbf{M}}_2 + \overline{\mathbf{M}}_3 + \overline{\mathbf{M}}_4 + \overline{\mathbf{M}}_5 \qquad (1)$$

where $\overline{\mathbf{M}}_i$ $(i = 0, 1, \cdots, 5)$ denotes the contributions, respectively, from underlying rough land-surface (0), scattering directly from canopy non-spherical scatterers (1), downward canopy scattering and then upward reflection from underlying surface (2), direct scattering from top snow layer covering the tree canopy (3), scattering directly from ice grains of snowpack (4), and

downward snow scattering and then upward reflection from underlying rough surface (5).

Using radiative transfer equation of dense media to obtain polarimetric scattering from snowpack, as follows,

$$\cos\theta \frac{d}{dz}\mathbf{I}(\theta,\phi,z) = -\kappa_e \mathbf{I}(\theta,\phi,z) + \mathbf{S}(\theta,\phi,z)$$

$$-\cos\theta \frac{d}{dz}\mathbf{I}(\pi-\theta,\phi,z) = -\kappa_e \mathbf{I}(\pi-\theta,\phi,z) + \mathbf{W}(\theta,\phi,z)$$

(2)

the solutions of $\overline{\mathbf{M}}_3, \overline{\mathbf{M}}_4, \overline{\mathbf{M}}_5$ are obtained. The attenuation through vegetation canopy as shown in Fig.1 will be added.

Using the first-order Mueller matrix solution of a layer of non-spherical particles above a rough surface, as a model of vegetation canopy, the solutions of $\overline{\mathbf{M}}_0, \overline{\mathbf{M}}_1, \overline{\mathbf{M}}_2$ are obtained.

Thus, numerical solution of $\overline{\mathbf{M}}$ of Eq. (1) is finally obtained to take account of all scattering and propagation through vegetation canopy, snowpack and underlying rough surface.

The parameters, such as the parameters H and α for target decomposition etc., are obtained for model simulation with different parameters, and are used for SAR data/image analysis.

3. DATA/IMAGE ANALYSIS

A pair of the parameters H-α has been well applied to the terrain surface classification. Fig. 2 shows H-α in a forest area of Northern China, DaXingAnLing in May 19 and November 19, 2007 from ALOS/PALSAR (L band) image data.

It can be seen that reducing fractional volume of leaves in deciduous forest in winter time (November) significantly shifts H-α to the pattern of random surface. Enhancement of multiple-scattering due to snowpack at L band is not significant. Deciduous tree and snow cover makes canopy more homogeneous,
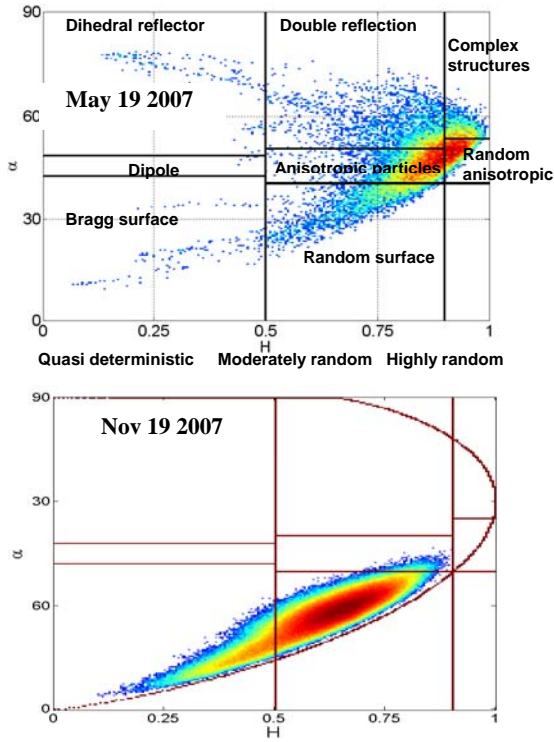
1

Fig. 2 *H-α* in a forest area in May 19 and November 19, 2007 from ALOS/PALSAR (L band) image data.

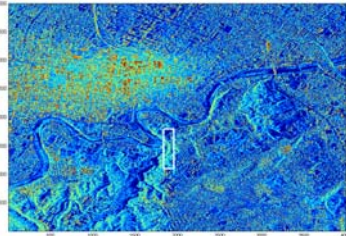Fig. 3 gives a PISAR image at X band, σ_{hh}, at Sendai test site.

Fig. 3 PISAR σ_{hh} image at X bands at Sendai test site

Fig. 4 gives *H-α* from the white rectangle area of Fig. 3 at L and X bands, respectively, where is forest area. Comparing two images of L and X bands, it is found that the distributions of *H-α* are much different at respective L and X bands, and the surface classification of *H-α* at L band image cannot be simply extended to X band image.
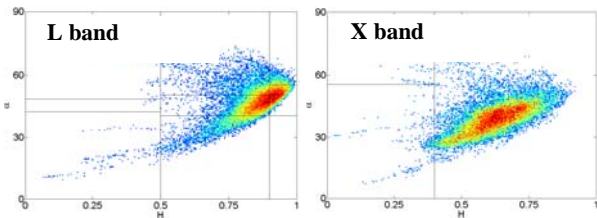

Fig. 4 PISAR images at L (left) and X (right) bands over forest canopy, respectively

It is interesting to see the correspondence between the images at L and X bands, as shown in Fig. 4. The respective regions with different colors, indicating quasi-deterministic, moderately random and highly random regions, at L band (a) are totally moved to different locations (with the same color) at X band (b-f), as shown in Fig. 5.
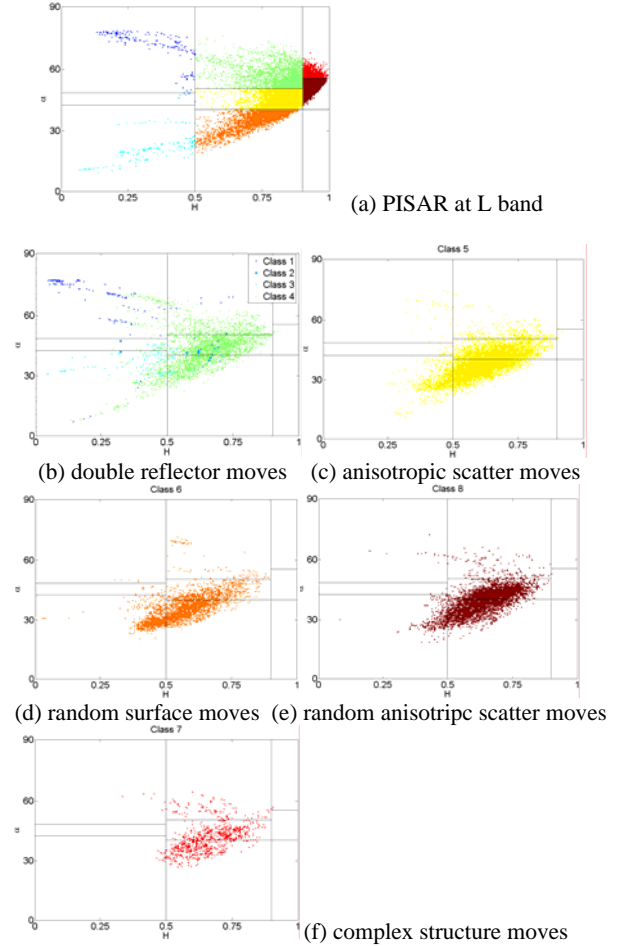

(a) PISAR at L band

(b) double reflector moves   (c) anisotropic scatter moves

(d) random surface moves   (e) random anisotripc scatter moves

(f) complex structure moves

Fig. 5 Transition of *H-α* as from L to X bands

It means that *H-α* classification is different for different frequency. This difference might be due to deeper penetration and more sensitivity of L band to whole inhomogeneity of scatter-canopy, where all double and triple volumetric scattering and surface scattering might be all involved to cause complicate scattering mechanism as the wave at L band more deeply penetrates into the canopy. As contrast, the wave at X band is more sensitive to the top layer, i.e. homogeneous leaves-canopy.

From numerical solution of $\overline{M}$ of Eq. (1) at L and X bands, *H-α* can be simulated for different parameters. As seen from Fig. 6, the red and pink lines show *H-α* at X band for a snowpack with depth d=100cm and incidence θ=30°, and changes for different parameters Δ and δ, which are defined in [2,3] to indicate the ratio of co-pol and cross-pol echoes. The green circle denotes *H-α* of

2

thick forest canopy. It can be seen that vegetation canopy causes large H due to randomness of canopy non-spherical scatterers with cross-pol increase.

As the media become ordered and homogeneous, H and α are reduced.
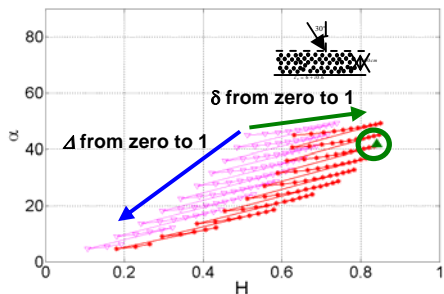

Fig. 6 Simulation of H-α classification for forest area with/without snow

Fig. 7 shows two PISAR images at L and X bands, respectively, in February 8, 2004, where there was snow in forest area.

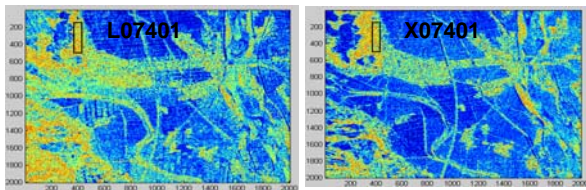Fig. 8 shows how H-α shifts in transition from L to X band.

Fig. 7 PISAR Data at L and X bands in Forest Area, Nagaoka 2004-02-08
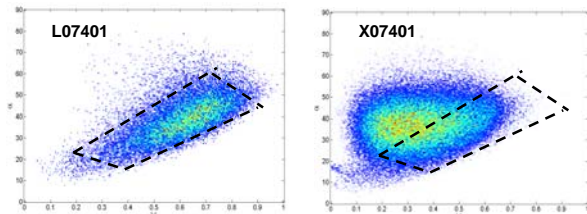

Fig. 8 Transition of H-α as from L to X bands in forest area

As snow covers the forest canopy, the PALSAR image at L band shows little effect from snowpack due to weak snow scattering. However, the image at X band shows significant effect due to snow scattering, and also moves H-α due to more canopy homogeneity.
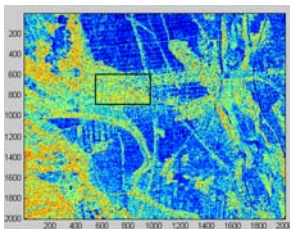

Fig. 9 PISAR Data at X bands in Residence Area, Nagaoka 2004-02-08

However, if the ROI (region of interest) is in residence area, e.g. indicated by a square in Fig. 9, the situation becomes more complicated.

Fig. 10 shows H-α of both L and X bands, which are not good matching to H-α surface classification catalogued in Fig. 1. In X band, much stronger scattering in residence area moves to α=45°, and angular bounces in residence buildings cause H reduced
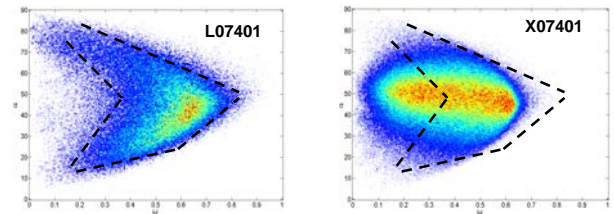

Fig. 10 Transition of H-α as from L to X bands in residence area

4.CONCLUSIONS

Using polarimetric scattering simulation of Mueller matrix solution of terrain surface with vegetation canopy and sow/no snow, some analysis of ALOS PALSAR and airborne PISAR images at L and X bands with H-α classification are discussed. It is found that

(1) Mueller matrix solution and H-α are linked with co-pol and cross-pol σ_{pq} and parsasmeters Δ and δ.

(2) L band cannot well detect snow in forest canopy.

(3) L band can see more inhomogeneity due to large penetration depth, and more randomness causes high H.

(4) X band can see snow due to high scattering.

(5) Snow makes the media more homogeneous, and reduces H-α at X band.

(6) H-αclassification at L band cannot be similarly extended to X band, It needs further study.

(7) More simulation with SAR data validation, and fusion at L,X bands need further study.

Another work on classification of typhoon-destroyed forest using PISAR data is also studied, and will be reported in future.

5. REFERENCES

[1] Y.Q. Jin, "Theoretical Modeling for Polarimetric Scattering and Information Retrieval of SAR Remote sensing", *Progress of Electromagnetics Research (PIER)*, 2010, 104: 333-384.

[2]. Y.Q. Jin, *Theory and Approach of Information Retrievals from Electromagnetic Scattering and Remote Sensing*, 2005, Berlin Heidelberg New York: Springer

[3] Y.Q. Jin and F. Xu, T*heory and Method of Polarimetric Scattering and SAR Remote Sensing Information*, 2008, Beijing: Science Press, in Chinese).